P_{b1} interface defect in thermal (100)Si/SiO_2: ^{29}Si hyperfine interaction

A. Stesmans, B. Nouwen, and V. V. Afanas'ev
Department of Physics, University of Leuven, 3001 Leuven, Belgium
(Received 8 April 1998)

An optimized electron spin resonance study has resulted in the observation of the full angular dependence of the hyperfine interaction spectrum associated with the unpaired electron of the P_{b1} point defect at the thermal (100)Si/SiO_2 interface, showing that the dominant interaction arises from a single ^{29}Si isotope. The hyperfine tensor exhibits nearly axial (weakly monoclinic I) symmetry with $A_{\|}$ ($\|\langle 211\rangle$) $=167\pm3$ G and $A_{\perp}=107\pm4$ G. Molecular-orbital analysis indicates that the unpaired electron resides for ~58% in a single unpaired Si hybrid orbital, found to be 14% *s* like and 86% *p* like, with the *p* orbital pointing closely along a $\langle 211\rangle$ direction at 35.26° with the [100] interface normal. If O is excluded as an immediate part of the defect, the results establish the kernel of the P_{b1} defect as a tilted (~22° about $\langle 011\rangle$) asymmetric, likely strained, $Si_3{\equiv}Si\bullet$ unit. Like P_b and P_{b0}, P_{b1} is a prototype Si dangling bond defect. All available structural information may, in principle, be compatible with the moiety being incorporated as part of a defected strained Si-Si dimer configuration at slightly subinterfacial position. The dimer has previously been advanced as a natural building block in matching SiO_2 to (100)Si. [S0163-1829(98)06440-6]

I. INTRODUCTION

The Si/SiO_2 unit remains a subject of intense research.[1–3] Without doubt, that interest mainly derives from the fact that it serves as the basic entity in the current most important technology for semiconductor device fabrication. But additionally, the unit also attracts much fundamental attention as a unique, easily grown structure for studying interface physics, that is, understanding how an amorphous solid (a-SiO_2) is naturally matched to a crystalline one (c-Si) within, at most, a few atomic layers.

However, while much of the electrical success of the Si/SiO_2 unit stems from the fact that the Si surface states are efficiently eliminated by growing a thermal oxide, the unit is not perfect. It was recognized early on electrically[4] that during thermal oxidation of Si, point defects are inherently generated at the interface as a result of lattice mismatch. Additionally, there also remain defects in the oxide.[3] As a result, the study of point defects has turned into one of the most important areas of investigation, boosted by the application of sensitive electrical techniques, which unveiled their electrical characteristics in impressive detail.[1–3] Yet, whatever their sensitivity, these electrical techniques, sensing charge aspects, inherently fall short of atomic identification. The latter, however, became within reach, at least in principle, upon the observation of interface defects by electron spin resonance (ESR),[5] a technique with atomic identification power, both structurally and chemically. In subsequent ESR work in conjunction with electrical measurements,[6,7] at least part of these defects were shown to be electrically active. They operate as trapping and/or recombination centers thus impairing crucial currents in adjacent Si layers, hence the high technological interest in atomic identification.

The appearance of the ESR-active interface defects, referred to as P_b-type centers, depends on the Si substrate orientation. A major property of these defects is that they crystallographically correlate with the Si substrate. At the bulk[8] (111)Si/SiO_2 interface, only one defect has so far been isolated,[2,9,10] specifically termed P_b. Mainly by ESR, it was convincingly identified[10] as a symmetric $Si_3{\equiv}Si\bullet$ unit, i.e., a trivalent interfacial Si backbonded to three Si's in the substrate, where the dot symbolizes the unpaired electron in an $sp^3_{\langle 111\rangle}$-like orbital. It exhibits C_{3v} symmetry and is ESR active when neutral. For this symmetry, four different orientations of identical defects in the Si lattice would occur. Yet, only the orientation with $p_{\langle 111\rangle}$ along the [111] interface normal is generally observed,[9–11] exposing its interface-constrained character.

The technological dominant (100)Si/SiO_2 structure, by contrast, exhibits two prominent ESR-active defects,[12] called P_{b0} and P_{b1}. For standard oxidation temperatures (800–950 °C), the naturally incorporated densities[2] of defect sites (passivated by H or not) are[13] $[P_b]\sim5\times10^{12}$ cm^{-2} and[14] $[P_{b0}]$, $[P_{b1}]\sim1\times10^{12}$ cm^{-2}. Referred to a single Si plane, this corresponds to fractional occupancies of 0.6 and 0.15%, respectively. The initial observations indicated lower than C_{3v} symmetry (C_{2v})—monoclinic I—for both defects, the P_{b0} symmetry, however, being nearly axial about $\langle 111\rangle$. Like P_b, both were initially[12] tentatively also ascribed to single unbonded interfacial Si orbitals, based on the similarities in ESR properties such as the principal g values tensor, the inherent character, and interfacial position. Generally, the atomic identification here is still less satisfactory or just absent, as ESR has so far failed to provide a set of data as complete and convincing as obtained for P_b in (111)Si/SiO_2. As compared to the P_b case, the reasons include the inherently lower defect density (~4 times) and spectral interference. In ESR context, atomic information about a point defect is inferred from the center's symmetry as contained in the g tensor and other useful ESR parameters such as line width and shape, and their temperature dependencies. However, the conclusive evidence must come from resolving the

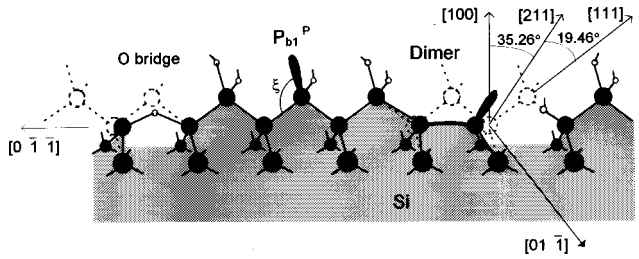

FIG. 1. Ball-and-stick models for P_{b1} at the (100)Si/SiO_2 interface including the initial P_{b1}^P model after Ref. 12, the strained defected Si-Si dimer model (SB1 model in Ref. 19) and the defected strained Si-O-Si bridge model (SB2 model in Ref. 19), with, for the latter two, the unpaired sp^3 hybrid adjusted along [211]. The dashed drawing represents the Si lattice before defect formation. The bonding angle ξ is also defined.

hyperfine (hf) interaction of the unpaired electron at the defect with nearby magnetic nuclei. The better set of data, including ^{29}Si hf structure, has been assembled[15,16] for P_{b0}, where a gaining impression[15,17] is that it just concerns the equivalent of the P_b defect, but now residing at (111)Si/SiO_2-like microfacets (steps) at the macroscopic (100)Si/SiO_2 interface. It would thus merely reflect nonideal (100)Si termination. The altered interface plane arrangement leads, as expected, to second-order variations in the defects nature as reflected in crucial ESR parameters, such as the g tensor, ^{29}Si hf interaction strength, inherent density, etc.[2,17]

II. P_{b1} DEFECT

The P_{b1} defect is still unidentified. Initially, Poindexter *et al.*[12] modeled P_{b1} as an interfacial $\equiv Si_2O$ entity (model P_{b1}^P in Fig. 1), the defect thus suggested to differ chemically from P_b and P_{b1}. Over the years, however, the model was countered partly experimentally,[18] but mainly theoretically.[19] The latter followed from a theoretical study of the P_{b1} defect, based on a combination of *ab initio* and semiempirical molecular orbital (MO) techniques. Detailed calculations were carried out on five model clusters, including the initial $\equiv Si_2O$ model and the SB1 model, the latter symbolizing an unpaired Si bond at one end of a strained reconstructed interfacial Si-Si dimer, i.e., $Si_2{=}Si^{\bullet}{-}Si{\equiv}Si_2O$, where the long hyphen represents the strained bond. The model originated from the Si-Si dimer, pictured as a natural strain-relief site[20,21] necessary to absorb strain in matching a-SiO_2 to (100)Si. Poindexter's model was found untenable based on the calculated electronic band gap level structure, being incompatible with the then available experiment result,[7] and effective correlation energy considerations. As to the SB1 model, the calculated electronic level structure was found close to the then available experimental data. But the model was also discarded as the predicted central ^{29}Si hf interaction was found to be too small. Yet, it should be added here that this conclusion was obtained by comparison to one singular experimental[18] value (for one orientation of the magnetic field), providing no information on the hf tensor symmetry and orientation. Hence, that conclusion may have appeared somewhat premature. If accepting the recent finding[14] that P_{b1} is not electrically active, i.e., no electrical levels deep in the Si band gap, we may face an upside-down situation for the SB1 model: indeed, it appeared initially acceptable on electrical grounds, but was discarded because of the predicted ^{29}Si hf values, while the reverse may be the case.

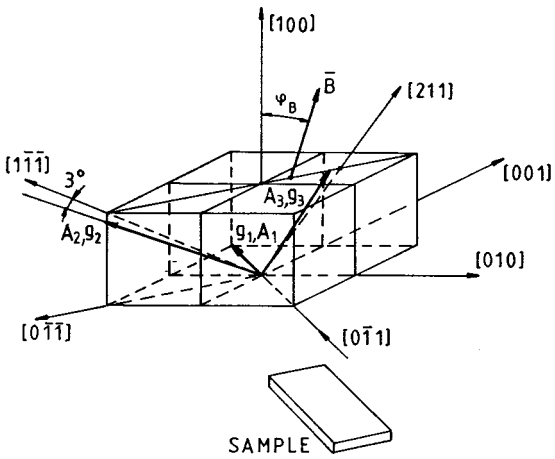

FIG. 2. Sketch of the P_{b1} g and hf tensor (A) principles axes within the cubic Si lattice for one of the four interface restricted equivalent defect orientations at the (100)Si/SiO_2 interface. The applied sample geometry is also shown.

The P_{b1} ESR properties[12] were recently accurately measured,[17] confirming the monoclinic I symmetry with $g_1 = 2.0058$, $g_2 = 2.00735$, and $g_3 = 2.0022$, where, importantly, the g_3 direction is at $3 \pm 1°$ (towards the [100] interface normal) with a ⟨211⟩ direction, the g_2 principal direction being approximately along ⟨111⟩, i.e., at $3 \pm 1°$ (towards the interface) with a ⟨111⟩ direction at 35.3° with the (100) interface plane. This is schematically shown in Fig. 2. Only the four crystallographic defect orientations (ESR-) equivalent through the 4 [100] face symmetry occur. From these results together with previous salient ESR data, the key part of P_{b1}, like P_b and P_{b0}, was also pictured as a single unpaired sp^3 hybrid on an interfacial Si. Furthermore, the former improved results on the g tensor and field-angle-dependent line broadening included a slight hint that the unpaired hybrid would point along the g_3 direction, i.e., closely along [211], instead of the g_2 direction (close to a normal ⟨111⟩ direction). But without supportive hf identification, the hint necessarily remained highly speculative.

The hf information on P_{b1} is scarce. There appear so far only two pertinent observations. In a first pioneering work[18] on standard thermal (100)Si/SiO_2 (900–1000 °C; 1.2 bar dry O_2; oxide thickness $d_{0x} = 10-500$ nm), a single—only for the applied magnetic field $\mathbf{B}\|\mathbf{n}$, the [100] interface normal—hf observation was reported for both P_{b0} and P_{b1}, tentatively attributed to ^{29}Si hf interaction. The observation was made on a sample stack containing 30–90 25-μm-thick (100)Si/SiO_2 slices of $\sim 23 \times 2.3$ mm^2 each. A hf splitting of $A_{[100]} \sim 157$ G was reported for P_{b1}, about 50 G larger than for P_{b0} ($\sim$105 G for $\mathbf{B}\|\mathbf{n}$), which in turn is comparable to that one of P_b ($\sim$117 G for $\mathbf{B}\|\mathbf{n}$). From this, it was speculated that the P_{b1} paramagnetic electron is highly localized on a single Si atom, and that the unpaired electrons are more tightly bound on P_{b1} centers than they are on P_{b0} defects. An important suggestion was that for all three defects, the hf interaction occurs with a single ^{29}Si. Unfortunately, however, these observations were restricted—very likely, for

TABLE I. Compilation of ^{29}Si hyperfine interaction parameters of the P_b and P_{b1} defects in various types of thermal (111) and (100)Si/SiO_2. The MO wave-function coefficients were calculated (Ref. 26) using $|\psi_{3s}(0)|^2 = 34.55\times10^{-25}$ cm^{-3} and $\langle r_{3p}^{-3}\rangle = 17.78\times10^{-24}$ cm^{-3} (cf. Ref. 28).

Defect	Reference	$A_{\parallel}$[a] (G)	$A_{\perp}$[b] (G)	$A_{B\|\|[100]}$ (G)	hf axis	No. equivalent sites	α^2	β^2	η^2[c]
				Bulk[d] thermal (111) and (100)Si/SiO_2 and SIMOX					
P_b	10	156±5	91±9	117	[111]	1	0.11	0.89	0.62
P_{b0}	18			105					
	24 (SIMOX)[e]	151	84	103	⟨111⟩	1	0.10	0.90	0.59
	25	144	72	102	⟨111⟩	1	0.09	0.91	0.66
	Current work	149±4	75±5	105±2	⟨111⟩	1	0.09	0.91	0.67
P_{b1}	Current work	167±3	107±4	156±2	∠[211],[f] $A_{\parallel}=3^0$	1	0.14	0.86	0.58
	18			157					
				Oxidized porous Si					
$P_{b(0)}$	15[g]	149–156	78–83		⟨111⟩	1	0.10	0.90	0.65
	16[h]	156	83		⟨111⟩	1	0.10	0.90	0.67

[a]No information on the sign of A is inferred; all A values are supposedly negative.

[b]Fitting monoclinic I symmetry results in $A_1(\|[0\bar{1}1]) = 102\pm3$ G; $A_2 = (\sim\|[111]) = 112\pm3$ G, and $A_3 = A_{\|} = 167\pm3$ G.

[c]It needs to be remarked that the inferred values of α^2, β^2, and η^2 depend on the used set of theoretical estimates for $|\psi_{3s}(0)|^2$ and $\langle r_{3p}^{-3}\rangle$. The derived values for α^2 and β^2 are almost invariant as these are a function of the *ratio* $\langle r_{3p}^{-3}\rangle/|\psi_{3s}(0)|^2$, for which the various theoretical estimates give about the same value (~0.51–0.53). However, η^2 depends on the *magnitude* of these wave function averages, so that the inferred value may significantly vary depending on the theoretical estimates used. For one, Brower (Ref. 10) using the values $|\psi_{3s}(0)|^2 = 25.84\times10^{-24}$ cm^{-3} and $\langle r_{3p}^{-3}\rangle = 13.68\times10^{-24}$ cm^{-3} (Ref. 37) found $\eta^2 = 0.82$ instead of 0.62 as quoted here.

[d]See Ref. 8.

[e]Confined Si/SiO_2/Si structure prepared by the method of ''separation by implantation of oxygen'' (SIMOX) starting from (111)Si or (100)Si.

[f][211] stands for [211], [2$\bar{1}$1], [$\bar{2}$11], and [$\bar{2}\bar{1}$1].

[g]Grown on (100)Si.

[h]Grown on (100)Si and (111)Si.

sensitivity reasons—to only the one observation for **B**‖**n**; it is the simplest ESR situation, as now the various signals for each type of defect (generally three for **B** rotating in the (011) plane] coincide, resulting in a two-line spectrum. Thus, the decisive information on the hf tensor symmetry and interaction strength remained still unknown, leaving the modeling undecided and providing a source for excessive speculation.

More recent information came from the study[22] of porous Si (PS), which, because of the strongly enhanced Si/SiO_2 interface area per unit sample volume (specific area ~300 m^2/cm^3), would enable drastic signal improvement in a typical ESR-sized sample. This has culminated in much research activity, mostly on P_{b0}, which, among others, has led to additional confirming data[15,16] on the P_{b0} ^{29}Si hf structure (cf. Table I). Interesting was the fact that one group,[15] studying mildly oxidized PS (1000 °C; 12 mbar O_2; 5–40 min) grown on (100)Si, reported the observation of the P_{b1} defect superposed on the generally dominant P_{b0} species, which opened new perspectives for P_{b1} hf structure exploration. However, while the P_{b0} ^{29}Si hf structure was again clearly observed, no P_{b1} hf structure could be traced, despite extensive research on numerous differently oxidized PS samples (oxide thickness $d_{0x} = 1-4$ nm)—in sharp contrast with Brower's observation. The authors concluded that the ^{29}Si P_{b1} hf structure remains unresolved from the Zeeman signal, putting an upper limit for the splitting at 40 G for **B**‖ [100], i.e., reduced by >60% as compared to P_{b0}. This left the P_{b1} hf story in dispute. Remarkably, the lack of any resolved P_{b1} hf structure observation was taken as evidence for the validity of a previously advanced SB1 model for the P_{b1} defect *(vide infra)*.

Clearly, conclusive P_{b1} identification is in need of hf structure information. This is the subject of the current work, reporting the successful observation of the full angular dependence of the dominant ^{29}Si hf structure, providing a fundamental clue as to the defect's microscopic structure. As a key inference, the results demonstrate that the P_{b1} unpaired electron resides in a single unpaired sp^3-like orbital, approximately oriented along a ⟨211⟩ direction.

III. EXPERIMENTAL TECHNIQUES

A. Samples

ESR-compatible samples of a 2×9 mm^2 main face were cut from a commercial 4-in-diam two-side polished (100)Si wafer (float zone; ~0.1 Ω cm; *p* type) about 29 μm thick, with the 9-mm edge along a ⟨011⟩ direction. After appropriate wet chemical cleaning, including a 10-min treatment in

H_2SO_4 (96%):H_2O_2(30%) [(4:1) by volume] at 80 °C and dipping for ~2 min at 22 °C in HF (39%):H_2O (1:9), the samples were submitted to three thermal steps. This was carried out using a high vacuum laboratory system equipped with a double-walled silica tube at the center of a mobile conventional electronically stabilized furnace, as described elsewhere.[13] First, they were thermally oxidized at 970 °C (1.1 atm O_2, 99.9995%, dry, d_{0x}~42 nm). Next, in order to maximize the P_{b1} density, the samples were submitted to hydrogenation (H_2, 99.9999%, 1 atm) at 795 °C for 1 h. As after such step, the major part of the P_b-type defects are left passivated by H (i.e., $P_{b(0,1)}$H formation), this was finally followed by a vacuum anneal at ~620 °C for ~1 h—a treatment known[14,23] to exhaustively depassivate (ESR activate) the P_b-type defects. Typically, an intensity ratio $[P_{b1}]/[P_{b0}] \approx 1.22$ is obtained, with $[P_{b1}] = (7.2 \pm 0.5) \times 10^{12}$ cm^{-2}. All the thermal steps were terminated by cooling to room temperature in an unaltered ambient. The cooling process occurs semiexponentionally with a time constant of ~200 and 390 s in vacuum and gas ambient, respectively. Typically, about 70 slices were stacked in an ESR sample.

B. ESR spectrometry

ESR measurements were carried out in the 1.6–4.3 K range employing a cw *K*-band (~20.09 GHz) spectrometer, as described elsewhere.[13] Routinely, it is driven in the adiabatic slow passage absorption mode, where modulation (~100 kHz; amplitude ~0.6 G) of the applied magnetic field **B** results in the recording of first derivative absorption signals. However, as weak hf structure detection was a main goal, the incident microwave power P_μ (~20 pW) was enhanced (P_μ~0.8 nW) to optimum signal magnitude, though without introducing excessive signal distortion. Under these partial saturation conditions, the rapid passage effects at 1.6 K resulted in recording undifferentiated absorptionlike peaks. **B** was rotated in the (011) plane with ϕ_B, the angle of **B** with the [100] interface normal **n**, varying from 0→90°. Spin densities were determined relative to a microsized Si:*P* intensity standard through double numerical integration of the dP_μ/dB spectra recorded in one trace. For spin-density calibration, spectra were measured in the undistorted mode in combination with intensified signal averaging (~200 scans), with the modulation field amplitude (~0.25 G) and P_μ (<20 pW) reduced to linear signal response levels.

C. Signal enhancement

As mentioned, the typical signal-to-noise ratio obtained in state-of-the-art ESR spectrometers is insufficient to allow the detection of P_{b1} hf structure in standard thermal (100)Si/SiO_2. The successful resolution of P_{b1} hf structure is seen to have resulted from cumulative signal enhancement in four ways: (1) maximizing the areal P_{b1} density by post-oxidation anneal in H_2; (2) enlarging the interface area comprised in an ESR sample stack to ~25 cm^2; (3) lowering of the observational temperature to 1.6 K in combination with optimization of the spectrometer detection mode; (4) intensive signal averaging (~100–200 scans).

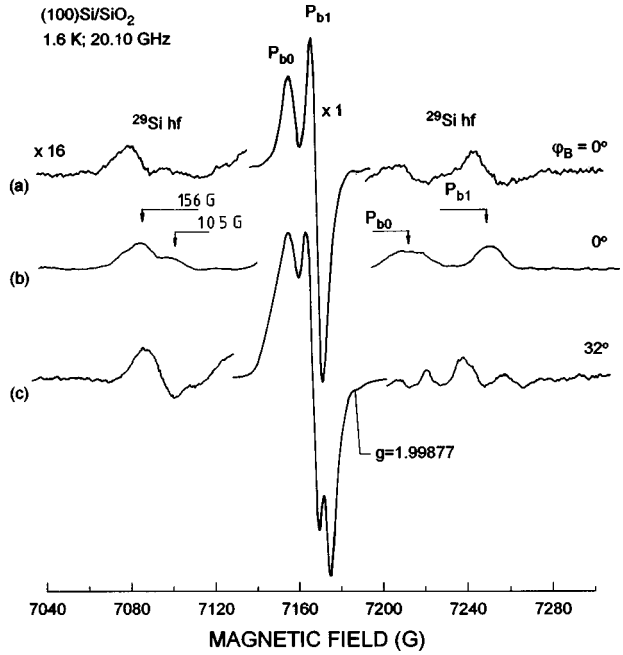

FIG. 3. Absorption derivative ESR spectra observed at 1.6 K under conditions of adiabatic slow passage (*a*,*c*; P_μ~20 pW) and rapid passage (*b*; P_μ~0.8 nW) in thermal (100)Si/SiO_2 grown at 970 °C (d_{ox}~42 nm) for two directions of **B** in the (011) plane; ϕ_B is the angle of **B** with the [100] interface normal. The spectra display the P_{b0} and P_{b1} Zeeman signals and resolved ^{29}Si hf structure. The angular dependent P_{b1} hf structure is clearly exposed.

IV. EXPERIMENTAL RESULTS AND ANALYSIS

A. Results

Typical ESR spectra observed in the slow passage low P_μ (undistorted) mode at 1.6 K are shown in Fig. 3 for two orientations of **B**. Though this detection is not the most sensitive one (not used generally for hf structure mapping), hf structure is clearly resolved next to strong P_{b0} and P_{b1} (central) Zeeman signals. The simplest spectrum occurs for **B**‖**n**, displaying pairs of hf doublets of splitting $\Delta B_{\rm hf}[100] = 105 \pm 2$ and 156 ± 2 G centered at the P_{b0} and P_{b1} Zeeman signals, respectively. The first one is the expected P_{b0} ^{29}Si hf structure, of splitting well in agreement with previous results.[10,24,25] The second doublet is assigned to P_{b1}. It was observed once before,[18] with identical splitting, and was tentatively ascribed to ^{29}Si P_{b1} hf structure. In the latter work, to maximize the *S*/*N* ratio, ESR was measured at <30 K in the dispersion mode under fast passage conditions giving absorptionlike signals. When measuring at higher P_μ under similar circumstances, our hf spectrum for **B**‖**n**—with enhanced *S*/*N* ratio–becomes indeed virtually identical to one of Brower (Fig. 4 of Ref. 18), as shown in Fig. 3(b), thus confirming that observation. The marked differences in signal features of the two hf doublets clearly indicates their dissimilar origin, i.e., P_{b0} and P_{b1}, thus justifying the assignment.

Unlike previous work, the achieved signal enhancement has enabled us to perform the full angular variation of the hf structure. This is exemplified in Fig. 3 also, where the P_{b1} hf structure is seen to split into various, generally three, components. This is as expected for P_{b1} as for **B** rotating in the

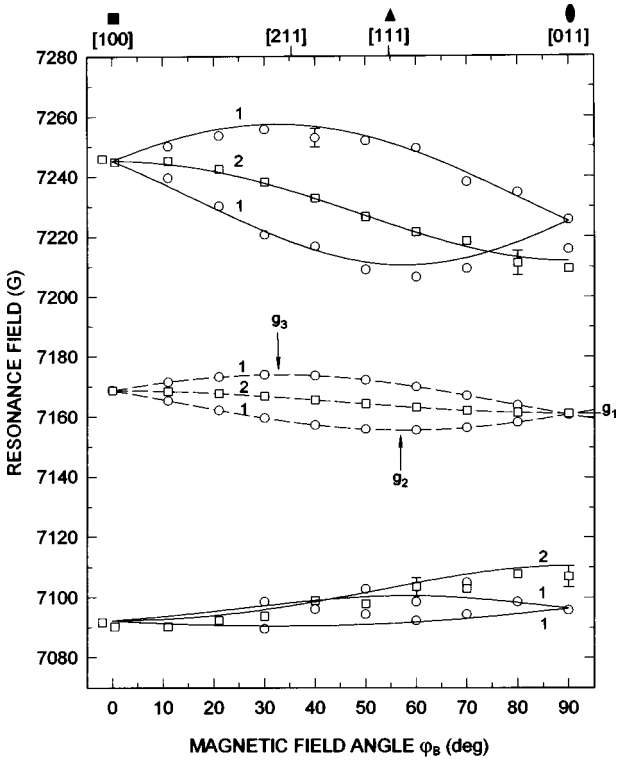

FIG. 4. Angular dependence of the P_{b1} ESR spectrum in bulk thermal (100)Si/SiO_2 for **B** rotating in the (011) plane (cf. Fig. 2). The squares represent hf signals of estimated double intensity as compared to those depicted by circles. The dashed curves represent the previously determined P_{b1} g map. The solid curves represent the optimized theoretical fit for monoclinic I (nearly axial) symmetry, from which the principal hf tensor values listed in Table I are inferred. The g and A tensor principal axes coincide within experimental accuracy. The various branches arise from identical defects, but differently oriented in the Si lattice. In both the g and hf (A) maps, only the four defect orientations equivalent through the $\bar{4}$-fold symmetry of the (100) face are observed. Numbers near the branches indicate relative intensities.

$(0\bar{1}1)$ plane, the g map exhibits three branches. As outlined previously, it exposes the fact that P_{b1}, exhibiting monoclinic I symmetry, is an interface constrained defect. In assigning the hf structure, also the relative intensity of the respective hf signals is informative. The three components of the P_{b1} hf structure exhibit different relative intensity, one being of approximately double intensity. Anticipating the interpretation, this factor has been incorporated in the P_{b1} hf mapping through the use of different symbols for the hf lines of estimated double intensity.

The inferred P_{b1} hf rotation pattern is shown in Fig. 4, together with the previously measured g pattern; hf signals of single and double intensity are symbolized by circles and squares, respectively. No other hf signals could be traced in a magnetic field window of ~500 G centered at the Zeeman signals, even after prolonged signal averaging.

The structural identification power of ESR bears on the observation of hf structure, which, in principle, enables the identification of the atom(s) on which the unpaired electron is predominantly localized, and in the most favorable case, to map the atomic structure of the defect. Next to the hf spectral composition and magnitudes of observed splittings, a key element in assigning hf structure is the relative signal intensities. As determined on undistorted low P_μ spectra, the ratio in spectral intensity (area under absorption curve) of the hf doublet to the Zeeman signal is found to be 0.044 ± 0.006 for P_{b1}. This agrees with the value of 0.049 expected for interaction with a single ^{29}Si (4.70% natural abundance) nucleus.

As is the case[10,17] for $P_{b(0)}$, the P_{b1} hf signals are broadened as compared to the Zeeman signal, e.g., for $\phi_B = 0°$, the peak-to-peak width ΔB_{pp} is 11.2 ± 0.4 and 4.0 ± 0.2 G for the hf and Zeeman signals, respectively. With the ratio of the absorption derivative peak-to-peak height ($2A_{pp}$) of the hf to the central signal measured as ~0.07, this refers to a difference in line shape. This is compatible with a Voigt signal of line shape factor $\kappa \equiv I/(A_{pp} \times \Delta B_{pp}^2) \sim 2.4$ for the Zeeman signal vs a Gaussian shape ($\kappa = 1.033$) for the hf signals.

Before addressing these hf results, it may be useful to add a remark on the extraction of the data, i.e., interpretation of the spectra. With two types of defects (P_{b0} and P_{b1}) simultaneously being observed, one may wonder about the discrimination and assignment of the respective, often interfering hf signals to either of the defects. Indeed, as known, the P_{b0} hf structure will generally also consist of three components for $\mathbf{B} \in (011)$. In addition to the higher relative P_{b1} density (i.e., $[P_{b1}]/[P_{b0}] \sim 1.22$), this was aided by three features. First, the width of the P_{b1} hf lines appears generally somewhat smaller than those of P_{b0}. Second, in gradually increasing P_μ, starting from the low-power undistorted detection mode, the enhancing rapid passage effect causes the P_{b1} hf signal to gain in relative prominence as a result of the unequal saturability; it enables spectrometer settings optimization for maximum P_{b1} resolution. Third, there is the recent observation[17] that the width of the P_{b0} Zeeman signal, as for P_b in (111)Si/SiO_2, is field angle dependent, which is predominantly (it may also contain some dipolar broadening) ascribed to a strain-induced Gaussian distribution in $g_\perp$ of spread $\sigma_{g\perp} \sim 0.0009$. P_{b1} exhibits a similar, though three times weaker effect. As this strain broadening is also reflected in the width of the corresponding hf lines, albeit relatively to a lesser extent, it will generally for an arbitrary orientation of **B** favor P_{b1} hf signal observation near P_{b0}.

Notwithstanding the fact that the P_{b0} hf signals are thus less prominent, the angular dependence of the P_{b0} hf structure was also measured. In agreement with previous reports,[15,24,25] its hf tensor is found to be axially symmetric about $\langle 111 \rangle$ with $A_\parallel$ ($\parallel \langle 111 \rangle$) $= 149 \pm 4$ G and $A_\perp = 75 \pm 5$ G.

B. MO analysis

The P_{b1} spectrum can be described[26,27] by the simplified spin Hamiltonian composed of the electronic Zeeman interaction and the hf interaction term

$$\mathcal{H} = \mu_B \mathbf{B} \cdot \mathbf{g} \cdot \mathbf{S} + \mathbf{I}_j \cdot \mathbf{A}_j \cdot \mathbf{S}, \tag{1}$$

with effective electron spin $S = \frac{1}{2}$. Here **g** is the electronic g dyadic, I the nuclear spin ($= \frac{1}{2}$ for ^{29}Si), and $\mathbf{A}_j$ the hf tensor for interaction of the electron spin with the jth nearby lattice site; for the present P_{b1} case, $j = 1$. Similar to the Zeeman g map, the hf structure pattern is found readily fitted with monoclinic I symmetry. The optimised fitting gives the principal hf tensor values A_1 ($\parallel [011]$) $= 102 \pm 3$ G, A_2

($\sim\|[111]$) $=112\pm3$ G, and A_3 ($\sim\|[211]$) $=167\pm3$ G. The departure from trigonal (axial) symmetry thus appears small. In fact, within experimental accuracy, the data are equally well fitted by axial symmetry, giving the values (see Table I) $A_\|=A_3=167$ G and $A_\perp=107$ G. To ease the discussion, we shall henceforth assume axial symmetry.

The fitting also indicates that the principal hf tensor axes coincide with those of the g tensor, which need not *a priori* be the case[27] (*vide infra*). However, while a satisfactory fit is obtained, the experimental accuracy does not permit to specify the A tensor principal directions to better than $\sim3°$. This finding strikingly demonstrates that within the simple picture of a single dangling bond at a $Si_3{\equiv}Si\cdot$ entity, the unpaired bond axis points closely along a $\langle211\rangle$ direction—not a normal $\langle111\rangle$ direction.

In the conviction that the unpaired P_{b1} electron resides in a Si orbital, the paramagnetic defect electron wave function $|\psi(\mathbf{x})\rangle$ may be approximated by a molecular orbital constructed as a linear combination of atomic sp^3 hybrids ψ_i centered on Si atoms near the defect

$$|\psi(\mathbf{x})\rangle=\Sigma_i\eta_i(\alpha_i|\psi_{s,i}(\mathbf{x})\rangle+\beta_i|\psi_{p,i}(\mathbf{x})\rangle), \tag{2}$$

where normalization requires $\Sigma_i\eta_i^2=1$ and $\alpha_i^2+\beta_i^2=1$. Here, η_i^2 is the wave function density at the ith site, and α_i^2 and β_i^2 give its relative s and p character. Because of its short range nature (ignoring overlap), the hf interaction of $|\psi(\mathbf{x})\rangle$ with nucleus i is dominated by the atomic orbital ψ_i at that site. Hence, to first order, the hf interaction will be axially symmetric along the p orbital lobe. For a singular broken sp^3 bond, the symmetry of the g and A tensor will be similar. The magnitude of the hf splitting can then directly be related to the defect wave function through the relations

$$A_\|=a+2b,\quad A_\perp=a-b, \tag{3}$$

where a and b, given as

$$\begin{aligned} a_i&=(\mu_0/4\pi)(8\pi/3)g\mu_B g_{\mathrm{N}_i}\mu_N|\psi_{s,i}(0)|^2\alpha_i^2\eta_i^2,\\ b_i&=(\mu_0/4\pi)(2/5)g\mu_B g_{\mathrm{N}_i}\mu_N\langle r_{p,i}^{-3}\rangle\beta_i^2\eta_i^2, \end{aligned} \tag{4}$$

represent the isotropic (s part: Fermi contact interaction) and anisotropic (p part: dipolar interaction) parts of the hf interaction. Here g_{Ni} is the nuclear g factor, μ_0 the vacuum permeability, μ_B the Bohr magneton, and μ_N the nuclear magneton. The values used for $|\psi_{s,i}(0)|^2$ and $\langle r_{p,i}^{-3}\rangle$ are those for neutral Si tabulated in Ref. 28. Though such linear combination of atomic orbitals (LCAO) approach is considered more interpretative than predictive,[29] the qualitative predictions are found largely correct, as, e.g., concluded from rigorous calculations[29,30] on the P_b defect. It was successfully applied[26,27] to point defects in c-Si.

The results of the LCAO analysis for the MO wave function parameters are compared with those of P_b and P_{b0} in Table I, where an overview of the ^{29}Si hf interaction parameters of P_b-type defects is presented. This provides useful information.

(1) It indicates that 58% of the paramagnetic orbital is localized on a single Si atom at the interface, with the hybrid exhibiting 14% s and 86% p character. These localization and sp hybridization values are quite similar to those found for prototype Si dangling bond defects such as, e.g., $G8$ (P-vacancy center) (Ref. 27) and P_b (Ref. 10; cf. Table I), leaving little doubt that the P_{b1} paramagnetic orbital also concerns a single Si dangling-bond orbital.

(2) Most revealing perhaps is that this unpaired Si hybrid points closely (within $\sim3°$) along a $\langle211\rangle$ direction at $\sim35°$ with **n**.

(3) The gyromagnetic and hf tensor symmetries are found to be identical within experimental accuracy. But, as mentioned, the accuracy on this statement cannot be better than $\pm3°$, e.g., the attained accuracy does not permit us to conclude that, e.g., the A_3 ($A_\|$) direction, like g_3, is really at $3\pm1°$ (towards the interface normal) with a $\langle211\rangle$ direction at $54.74°$ with the interface plane. However, to simplify the wording, we shall henceforth assume both tensor symmetries to be coinciding.

(4) If deemed significant, the P_{b1} unpaired hybrid displays slightly more s character than the P_{b0} one. The simple MO theory gives the relationship[31] between the hybridization ratio α^2/β^2 of the dangling bond and the angle ξ it makes with the adjacent sp^3 backbond orbitals as $\cos\xi=-[\alpha^2/(3-\beta^2)]^{1/2}$. According to this formula, the P_{b1} defect Si atom, at the apex of a $\equiv Si\cdot$ tetrahedron, is in average ~0.067 Å more remote from the plane of the three back neighbors (less planar) as compared to P_{b0}.

Within the LCAO framework, the results must imply that the key part of P_{b1} consists of a tilted $\equiv Si_0$ entity that, under interfacial physicochemical influence, has rotated (cf. Fig. 1) about a $\langle011\rangle$ axis over $\sim22°$ so as to bring the Si dangling bond from its normal $\langle111\rangle$ direction towards a nearest $\langle211\rangle$ direction.

This finding on the unpaired sp^3-like hybrid direction makes previous results transparent. First, there are the measured g shifts[12,17] $\Delta g\equiv g-g_{\mathrm{fe}}$, where $g_{\mathrm{fe}}=2.002\,32$ is the free electron g value. The shift is smallest, i.e., $-0.000\,12$ (close to zero), along the [211] g_3 principal direction, while the shift is substantially larger and of comparable magnitude (i.e., 0.005 and 0.0035) along the other two principal g directions. In line with the current finding that the unpaired P_{b1} hybrid points along the g_3 direction, the successful g shift interpretation[26] for a single broken Si orbital based on simple MO theory indeed predicts to first-order zero g shift for $g_\|$ and a positive, order of magnitude larger shift in $g_\perp$. Second, the inferred dangling bond direction (g_3 direction) is also corroborated by the recently revealed[17] strain-induced angular dependent part in the P_{b1} linewidth. It was found smallest (possibly absent) along the g_3 direction. This again is consonant with the simple[26,32] MO view, predicting that, to first order, the strain-induced variations in bond lengths and angles near the defect site only lead to a distribution in $g_\perp$, none in $g_\|$, however. Hence, the broadening is also minimal along the sp^3 hybrid (g_3) direction.

V. DISCUSSION

A. P_{b1} characteristics

With the basic atomic unit of P_{b1} identified, a main goal of this research has been accomplished. It now remains to trace how the entity is incorporated as part of a larger defect structure. That structure, placed in an adequately chosen, suf-

ficiently extended Si/SiO_2 cluster will enable reliable theoretical verification through quantum-mechanical calculation. Defect modeling can only be considered definite after successful theoretical support. Together with the newly gained hf information, this search should be guided by the salient experimental facts, mostly inferred by ESR. It may be noticed that in addressing the identity of P_{b1}, its properties are often compared with those of the other unavoidably copresent prominent ESR-active defect P_{b0}. When referring to our knowledge of the P_{b0} defect, this may appear beneficial. Salient P_{b1} facts include:

(1) The P_{b1} g tensor data show that P_{b1} is an interface restricted[12,17] defect of monoclinic I symmetry. The lowest principal g value $g_3=2.0022$ is only weakly shifted from $g_{\rm fe}$. This g_3 axis is at $3\pm1°$ (towards the interface normal) with a $\langle 211\rangle$ direction at 35.26° with the [100] interface normal, while the principal g_2 (=2.007 35) is at 3° with $\langle 111\rangle$.

(2) The magnet angle dependent line broadening,[17] ascribed to a strain-induced distribution predominantly in $g_\perp$, is smallest (absent) for $\mathbf{B}\|g_3$ axis [211]. The overall angular dependent broadening is significantly weaker (~3 times) than for $P_{b(0)}$, which would indicate the P_{b1} defect to reside in a more regular (less strained) environment.

(3) The P_{b1} center is more sensitive to saturation[17] than P_{b0}; ~3 times in terms of P_μ. In one view, this may indicate that as compared to P_{b0}, the P_{b1} defect, in terms of spin-lattice relaxation, responds more to the Si lattice than to the a-SiO_2 network. If simply connected with the defect's location, it would suggest P_{b1} to be at a slightly more subinterface plane position in the substrate.

(4) The study[18] of ^{17}O enriched $(100)Si/SiO_2$ indicates that O is not an immediate part of the P_{b1} defect. Only some ^{17}O-induced ESR line broadening (~3.5 G) is observed, attributed to the interaction on the unpaired spin with the remote O cloud in the overlaying oxide. With no hydrogen hf observed, H is also excluded as a building block of the defect.

(5) The activation energy for passivation in *molecular* H was found to be close[33,34] for all three defects, P_{b0}, P_{b0}, and P_{b1}. The former two exhibit an identical value, i.e., $E_a=1.51\pm0.04$ eV, while $E_a(P_{b1})=1.57\pm0.04$ eV is found slightly higher, however. This finding in itself was taken as a significant indication that the P_{b1} defect, like P_b, also concerns an unpaired single sp^3 hybrid at an interfacial Si, even apart from other evidence.

(6) Passivation in atomic H, by contrast, occurs different,[35,36] P_{b1} defects being more readily passivated than P_{b0}. The behavior of P_{b0} appears consistent with the balance expected[35] from the simple picture inferred for the P_b-H_2 interaction kinetics.[23,33] Likely, this dissimilarity is to be related with the actual local positioning of the respective defects and their immediate environment, e.g., in the case of P_{b0}, the possible proximity of H-scavenging defects (sites).

(7) The electrical role of P_{b1} is in dispute. From straightforward ESR experiments, based on sample sets exhibiting systematic significant differences in $[P_{b1}]$, we concluded[14] the center not to be active as an electrical interface trap, implying that there are no +/0 and 0/− charge transition levels deep in the Si gap. This contrasts with the initial experiment,[7] which concluded P_{b1} to be a deep amphoteric adverse interface trap with the +/0 and 0/− transition levels, respectively, at +0.45 and +0.8 eV above the valence-band edge deep in the Si gap.

B. P_{b1} configuration

As to possible configurations comprising the P_{b1} entity, the inferred hf data are selective. For instance, it eliminates at once all suggestions based on an $\equiv Si_0$ unit *regularly* incorporated into c-Si. If still needed, it also excludes P_{b1} to constitute an unpaired electron trapped in a molecular Si-Si bent bond, e.g., at the site of a Si vacancy, for various reasons. (1) In such case, the ^{29}S hf interaction would primarily be with two equivalent Si sites, rather than one. (2) As the g tensor should reflect the symmetry of this molecular reconstructed bond, the [100] axis should be a principal g symmetry axis, unlike observations. (3) The defect would be charged when ESR active.

Perhaps in a simplest scheme, the basic P_{b1} unit may be pictured incorporated as one half of a $Si_2{=}Si^{\bullet}$-Si≡ defected dimer configuration at slightly subinterfacial position (see Fig. 1). As a result of the pulling of the two interfacial next-nearest-neighbor Si atoms together under influence of surrounding strain during the Si-Si bond reformation, the $Si_2{=}Si^{\bullet}$—moiety with the left broken bond may be envisaged as having tilted about the [011] axis over ~20° away from [111] towards the [100] interface normal, the unbonded hybrid now pointing approximately along [211]. (In Fig. 1, such dimer configuration is sketched as having formed after the removal of two next-nearest-neighbor Si surface atoms. Practically, the defect might occur as a special strained dimer at the edge of single height steps S_B bordering a terrace.[38]) It may be remarked that according to this picture, it is rather coincidental that the principal g_2 axis points nearly along [111].

If placed slightly subinterfacial so that the defect structure is rigorously fixed by the Si lattice without much disturbance from the top SiO_2 network, this picture could, at least in principle, account for the various salient experimental facts thus far accumulated: The symmetry axes of the unpaired orbital at such tilted $Si_3{\equiv}Si^{\bullet}$—entity, i.e., [011], ~[211], and ~[111], agree with the measured principal g axis (cf. Figs. 1 and 2). Also according to this symmetry, three different principal g value magnitudes are expected, that is, lower than axial symmetry of g. Since the unpaired sp^3-like hybrid points along the g_3 axis (~[211]), the g shift along [211] is an order of magnitude smaller than along the two other perpendicular directions, as observed. As the unpaired spin resides in a single dangling sp^3-like hybrid, the g and hf tensor symmetries are expected to coincide to first order, also in agreement with observations.

C. P_{b1} theoretical assessment

The strained fully bonded Si-Si dimer had previously been proposed as a natural building block in matching SiO_2 to (100)Si, accounting for the observed Si^{1+} oxidation state at the interface.[20,21] As mentioned though, initial calculations concluded the dimer model for P_{b1} to be untenable. Perhaps,

improved calculations on a more reprensative cluster incorporating the dimer at a subinterfacial level may provide more insight.

Recently, Edwards has theoretically readdressed the several models for P_{b1} explored before.[39] In particular, the previous semiempirical MO calculations,[19] using MINDO/3, were repeated in an *ab initio* unrestricted Hartree-Fock approach with allowance for *more* defect *relaxation*. From the models considered, they concluded that only the SB1 and $P_{b1\text{-H}}$ (the original P_{b1}^{P} model with the O atom faced by the unpaired Si bond replaced by H) could be kept as candidates. Focussing on SB1, *ab initio* calculations were performed with basically two new elements: (1) a significantly smaller cluster was considered, where all atoms were allowed to relax; (2) *d* functions were included in the used valence basis set. As described, this resulted in two main variations: (1) reduction of the equilibrium length of the strained Si-Si bond from 2.52 to 2.35 Å, i.e., the regular Si-Si bond length in Si. It may be noticed that the defect would now rather look like a regular P_b entity, of which the known magnitudes of the A values (cf. Table I) will indeed be in the range of those reported for P_{b1}; (2) Significant increase of the central ^{29}Si hf interaction, now given as $A_1=115.4$ G, $A_2=119.9$ G, and $A_3=186.2$ G—much closer to the present experimental P_{b1} ^{29}Si hf data, indeed (cf. Table I). It would credit the SB1 model. However, it remains to be seen whether the theoretical ''improvements'' with respect to the experimental data are not merely fortuitous: The calculations are performed on a very small cluster, with no consideration of the effect of the top (SiO_X) coverage. Next, the calculations predict two electrical levels in the Si band gap, in sharp contrast with recent data.[14] Also, the relaxed unpaired Si-bond orientation remains unspecified.

But, however attractive the dimer picture, other structures may be envisaged. Based on symmetry considerations, also of interest is the $Si_2{=}Si^{\bullet}$-O-Si≡ oxygen bridge strain relief center (termed SB2 in Ref. 19). Like the dimer, it is also considered as a natural strain relief center in matching c-Si to a periodic form (e.g., tridymite) of SiO_2. Based on symmetry properties, even the initial Poindexter P_{b1}^{P} model may be reconsidered. Yet, while both models may display an acceptable symmetry, they are likely to be untenable on the basis of theoretical calculations of the electric level positions in the Si band gap and the incorporation of O as an essential building block (O back bond).

Finally, it needs to be commented on the dissonant results on porous[22] (100)Si, where no ^{29}Si P_{b1} hf structure could be observed despite the intense Zeeman signal and intensive search on various samples. As the reported g tensor data indicate, the failure cannot have resulted from having measured a defect different from P_{b1}. As already hinted before,[17] one possibility may originate from the generally greater sensitivity of hf interactions than the Zeeman line to strain and disorder.[10] In view then of the admixed Si/SiO_2 interface nature in PS *vis-à-vis* bulk (100)Si/SiO_2, the P_{b1} hf structure may have remained undetected as a result of excessive line broadening.

VI. CONCLUSIONS

An ESR study was carried out at cryogenic temperatures on conventional thermal (100)Si/SiO_2. Optimization of ESR spectroscopy has resulted in the full angular mapping of the strong ^{29}Si hf interaction associated with the P_{b1} defect in thermal (100)Si/SiO_2. The data show that the hf structure results from interaction with a single ^{29}Si isotope. The hf tensor exhibits nearly axial (weakly monoclinic I) symmetry about ⟨211⟩, with $A_{\parallel}=167\pm3$ G and $A_{\perp}=107\pm4$ G. Like the g map, the hf structure map also exhibits three branches (three pairs of doublets) for **B** in the (011) plane, arising from identical but differently oriented P_{b1} defects in the Si (surface) lattice. It affirms P_{b1} as an interface constrained defect.

Analysis based on the LCAO approach demonstrates that the paramagnetic P_{b1} electron is localized for ~58% in a single sp^3 hybrid; It is 14% s like and 86% p like, with the p orbital approximately pointing along a ⟨211⟩ direction at ~35° with the [100] interface normal.

The P_{b1} defect is convincingly identified, like P_b, as a prototype Si dangling bond (≡$Si^{\bullet}$ tetrahedron) defect. Combination with the previous conclusion[18] excluding O as an immediate part of the P_{b1} defect reveals it as a ⟨211⟩ oriented (~20° tilted), likely strained, $Si_3{\equiv}Si^{\bullet}$ unit. Clearly, thorough theoretical analysis will be required to trace the way how this unit is incorporated in a larger defect structure. It is felt that with the currently provided hf data, this can now be reliably carried through so as to culminate in the definite model.

The present results complete the identification of the ESR-active defects at the Si/SiO_2 interface. With inclusion of the similarity of P_{b0} and P_{b1}, it now appears that the kernel of all three defects, P_b, P_{b0}, and P_{b1}, is *chemically* identical; $^{\bullet}Si{\equiv}Si_3$ is the generic entity of the three defects. Yet, they do differ *physically*: First, there are second-order differences between P_{b0} and P_b related with their positioning at two macroscopically differently oriented interfaces; second, there is a major (orientational) difference between the former two defects and P_{b1}. It are these particular physical differences (e.g., regarding orientation, bond strain, structural relaxation) that account for the observed spectroscopical and interactive dissimilarities.

So, if, in an easygoing way, one would refer globally to all three defects just as singular Si dangling bond defects, it would imply gross oversimplification, covering only part of the physical reality. More refined terminology may be required. For P_b and P_{b0}, the single unpaired Si sp^3 hybrid points along a normal ⟨111⟩ direction, while it points nearly along ⟨211⟩ (within 3°) for P_{b1}; in short then, the defects may be referred to as ⟨111⟩ and ⟨211⟩ oriented $^{\bullet}Si{\equiv}Si_3$ defects, respectively. In the particular case of P_{b1}, it must be remembered though that the three Si backbonds are not equivalent.

[1] For a review on Si/SiO_2 defect physics, see the 13 papers in Semicond. Sci. Technol. **4**, 961 (1989), and references therein.
[2] E. Poindexter and P. Caplan, Prog. Surf. Sci. **14**, 211 (1983).
[3] R. Helms and E. Poindexter, Rep. Prog. Phys. **57**, 791 (1994).
[4] D. M. Brown and P. V. Gray, J. Electrochem. Soc. **115**, 760 (1968).
[5] Y. Nishi, Jpn. J. Appl. Phys. **10**, 52 (1971).
[6] E. H. Poindexter, G. J. Gerardi, M.-E. Rueckel, P. J. Caplan, N. M. Johnson, and D. K. Biegelsen, J. Appl. Phys. **56**, 2844 (1984).
[7] G. J. Gerardi, E. H. Poindexter, P. J. Caplan, and N. M. Johnson, Appl. Phys. Lett. **49**, 348 (1986).
[8] The notion ''bulk'' refers to conventional Si/SiO_2 thermally grown starting from Si wafers, and is used here to discriminate with less conventional $(111)Si/SiO_2$ structures as, e.g., encountered in SIMOX and porous Si.
[9] P. Caplan, E. Poindexter, B. Deal, and R. Razouk, J. Appl. Phys. **50**, 5847 (1979).
[10] K. Brower, Appl. Phys. Lett. **43**, 1111 (1983).
[11] A. Stesmans, Appl. Phys. Lett. **48**, 972 (1986).
[12] E. Poindexter, P. Caplan, B. Deal, and R. Razouk, J. Appl. Phys. **52**, 879 (1981).
[13] A. Stesmans, Phys. Rev. B **48**, 2418 (1993).
[14] A. Stesmans and V. V. Afanas'ev, J. Phys.: Condens. Matter **10**, L19 (1998).
[15] H. J. von Bardeleben, D. Stievenard, A. Grosman, C. Ortega, and J. Siejka, Phys. Rev. B **47**, 10 899 (1993); H. J. von Bardeleben, M. Schoisswohl, and J. L. Cantin, Colloids Surf., A **115**, 277 (1996).
[16] F. C. Rong, J. F. Harvey, E. H. Poindexter, and G. J. Gerardi, Appl. Phys. Lett. **63**, 920 (1993).
[17] A. Stesmans and V. V. Afanas'ev, J. Appl. Phys. **83**, 2449 (1998).
[18] K. L. Brower, Z. Phys. Chem., Neue Folge **151**, 177 (1987).
[19] A. H. Edwards, in *The Physics and Chemistry of SiO_2 and the SiO_2 Interface*, edited by C. R. Helms and B. E. Deal (Plenum, New York, 1988), p. 271.
[20] A. Ourmazd, D. W. Taylor, J. A. Rentschler, and J. Bevk, Phys. Rev. Lett. **59**, 213 (1987).
[21] A. Pasquarello, M. S. Hybertsen, and R. Car, Phys. Rev. Lett. **74**, 1024 (1995).
[22] J. L. Cantin, M. Schoisswohl, H. J. von Bardeleben, N. H. Zoubir, and M. Vergnat, Phys. Rev. B **52**, R11 599 (1995).
[23] K. L. Brower, Phys. Rev. B **42**, 3444 (1990).
[24] W. E. Carlos, Appl. Phys. Lett. **50**, 1450 (1987).
[25] J. W. Gabrys, P. M. Lenahan, and W. Weber, Microelectron. Eng. **22**, 273 (1993).
[26] G. D. Watkins and J. W. Corbett, Phys. Rev. **121**, 1001 (1961).
[27] G. D. Watkins and J. W. Corbett, Phys. Rev. **134**, A1359 (1964).
[28] J. R. Morton and K. F. Preston, J. Magn. Reson. **30**, 577 (1978).
[29] M. Cook and C. T. White, Phys. Rev. B **38**, 9674 (1988).
[30] A. H. Edwards, Phys. Rev. B **36**, 9638 (1987).
[31] C. A. Coulson, *Valence* (Oxford University Press, London, 1961), p. 203.
[32] K. L. Brower, Phys. Rev. B **33**, 4471 (1986); A. Stesmans and J. Braet, in *Insulating Films on Semiconductors*, edited by J. J. Simonne and J. Buxo (Elsevier, Amsterdam, 1986), p. 25.
[33] K. L. Brower, Phys. Rev. B **38**, 9657 (1988).
[34] A. Stesmans, Appl. Phys. Lett. **68**, 2076 (1996); **68**, 2723 (1996).
[35] J. H. Stathis and E. Cartier, Phys. Rev. Lett. **72**, 2745 (1994).
[36] K. Vanheusden, W. L. Warren, W. M. Shedd, R. D. Pugh, D. M. Fleetwood, J. R. Schwank, and R. A. B. Devine, in *Proceedings of the 1997 IEEE SOI Conference, Fish Camp, 1997* (IEEE, New York, 1997), p. 64.
[37] K. L. Brower, Phys. Rev. B **26**, 6040 (1982).
[38] Y. H. Xie, G. H. Gilmer, C. Roland, P. J. Silverman, S. K. Buratto, J. Y. Cheng, E. A. Fitzgerald, A. R. Kortan, S. Schuppler, M. A. Marcus, and P. H. Citrin, Phys. Rev. Lett. **73**, 3006 (1994).
[39] J. H. Stathis, E. Cartier, A. H. Edwards, and E. H. Poindexter, in *Silicon Nitride and Silicon Dioxide Thin Insulating Films*, edited by M. J. Deen, W. D. Brown, K. B. Sundaram, and S. I. Raider (Electrochemical Society, Pennington, NJ, 1997), p. 259.